

# Measurement-Based Analysis of Millimeter-Wave Channel Sparsity

William Sloane, Camillo Gentile <sup>✉</sup>, Mansoor Shafi <sup>✉</sup>, *Life Fellow, IEEE*, Jelena Senic <sup>✉</sup>,  
 Philippa A. Martin <sup>✉</sup>, *Senior Member, IEEE*, and Graeme K. Woodward <sup>✉</sup>, *Senior Member, IEEE*

**Abstract**—Millimeter-wave (mmWave) channel sparsity is widely exploited to reduce the complexity of compressed sensing and beamtracking algorithms for 5G, yet there are still many misconceptions about it: that it arises from pencilbeam antennas admitting just a few paths, that the channel in fact has just a few paths, and that the channel is always sparse. What is missing to confirm these conjectures is a measurement-based analysis, to our knowledge conducted by only two papers thus far, however, both at *microwave* (5 GHz), in a single environment, and based on just a few ( $\leq 49$ ) measurements. For conclusive analysis on *mmWave* sparsity, we have collected measurements with our high-resolution 3-D double-directional 60 GHz channel sounder in three indoor and two outdoor environments, comprising a total of 750 measurements while investigating both line-of-sight (LoS) and obstructed LoS (OLOs) conditions. We learned that in LoS, the channel is always sparse that sparsity drops notably from LoS to OLoS and that mmWave sparsity is inherent to the channel itself—not to pencilbeam antennas—since our sounder has omnidirectional field-of-view. We also propose a sparsity metric that accounts for channels with just a few paths, which we found to occur in some environments.

**Index Terms**—60 GHz, channel modeling, Gini index,  $k$ -factor, spatial degrees of freedom (DoF).

## I. INTRODUCTION

THE foregone conclusion of millimeter-wave (mmWave) channel sparsity is widely cited throughout the literature [1], [2], [3] and exploited to reduce the complexity of compressed sensing, beamforming, and beamtracking algorithms for 5G [4], [5], [6]. Its sparsity stems from large diffraction losses due to the narrowing of the Fresnel zone at such short wavelengths [7], [8], [9], [10], leaving direct transmission and specular reflection [11] as the chief mechanisms for propagation between the transmitter (T) and receiver (R). This translates to just a few dominant propagation paths detected at R; indeed, measurements at 28, 60, and 83 GHz in [9] and [12] demonstrate that the line-of-sight (LoS) path can constitute up to 75%

of the R power while on average diffracted paths accounted for only 1%. The measurements in [13] show that when the LoS is blocked, several dominant reflected paths act as the main propagation mechanisms due to the lack of diffraction. While some agree with this definition of sparsity [1], [14], [15]—that most of the R power will be concentrated in just a small subset of detected paths—others loosely define a sparse channel as one that exhibits little multipath richness [2]. Yet others claim that all wireless channels—microwave, mmWave, and above—are sparse because practical systems lack sufficient bandwidth, beamwidth, and/or dynamic range to resolve all the paths [16], [17], [18]. Although it is suggested in [19] and [20] that sparse channels only have a few clusters—supported by measurements in [21] and [22]—the mmWave models in [12], [23], and [24] indicate otherwise. Still others [25] do not even attribute mmWave sparsity to the channel, but rather to practical 5G systems requiring highly directional pencilbeam antennas, which admit just a few paths. Indeed, a universally accepted definition of mmWave sparsity is still elusive.

This is because only two papers, to our knowledge, have conducted the measurement-based analysis of channel sparsity to date, albeit at *microwave*: In [18] and [26], a total of 26 measurements at 5.2 GHz were used to perform analysis in a single indoor environment; in the analysis, the channel is represented through a four-dimensional matrix consisting of angle-delay-Doppler bins and the channel is deemed sparse if the number of bins with significant power lies below a threshold. The analysis in [14] and [15] at 5.9 GHz is much more comprehensive, in that three metrics<sup>1</sup> for sparsity are considered—1) the Gini index, 2) the Spatial Degrees of Freedom (DoF), and 3) the Rician  $K$ -Factor—and the correlation between the three is computed.

In this letter, we conduct a comprehensive measurement-based sparsity analysis similar to [14] and [15]; however, the following statements hold.

- 1) For the first time at *mmWave* (60 GHz), demonstrating that the channel is, indeed, much sparser than at *microwave*.
- 2) Instead of a single outdoor environment, we consider three indoor and two outdoor environments—by the same (NIST) authors for unbiased comparison—demonstrating that sparsity can vary significantly across environments.
- 3) Instead of LoS conditions alone, we consider both LoS and obstructed LoS (OLOs) in each environment. OLoS—when the LoS path is blocked by humans, buildings, foliage, etc.—is faced often at mmWave due to much greater

<sup>1</sup>We also considered the number of paths as a fourth metric but found it to be a poor indicator.

Manuscript received 24 October 2022; revised 15 November 2022; accepted 23 November 2022. Date of publication 28 November 2022; date of current version 7 April 2023. (*Corresponding author: Camillo Gentile.*)

William Sloane is with the National Institute of Standards and Technology (NIST), Gaithersburg, MD 20899 USA, and also with the University of Canterbury, Christchurch 8041, New Zealand (e-mail: william.sloane@nist.gov).

Camillo Gentile and Jelena Senic are with the National Institute of Standards and Technology (NIST), Gaithersburg, MD 20899 USA (e-mail: camillo.gentile@nist.gov; jelena.senic@nist.gov).

Philippa A. Martin and Graeme K. Woodward are with the University of Canterbury, Christchurch 8041, New Zealand (e-mail: philippa.martin@canterbury.ac.nz; graeme.woodward@canterbury.ac.nz).

Mansoor Shafi is with Spark NZ, Wellington 6011, New Zealand (e-mail: mansoor.shafi@spark.co.nz).

Digital Object Identifier 10.1109/LAWP.2022.3225246

TABLE I  
MEASUREMENT AND ENVIRONMENTAL PARAMETERS

	<i>Lobby</i>	<i>LR</i>	<i>Hallway</i>	<i>Pathway</i>	<i>Street</i>
T/R height (m)	2.5/1.6	2.5/1.6	2.5/1.6	2.5/1.6	4/3.5
No. R locations	200	290	130	60	70
T-R distance (m)	6–11	6–14	8–60	6–25	19–100
Avg. no. of paths	62	85	31	15	73

penetration loss than at microwave, and we demonstrate that sparsity can drop notably from LoS to OLoS.

- 4) Instead of 49 measurements, we collect a total of 750 large-scale measurements for conclusive analysis.
- 5) We propose a corrected Gini index to account for when the number of paths is few—which we found to occur in some environments—and demonstrate that it drastically improves the correlation between the three sparsity metrics.

In Section II, we summarize our measurements followed by Section III, which presents the three sparsity metrics, including the corrected Gini index. Section IV compares the three metrics per environment and discusses key factors in mmWave sparsity.<sup>2</sup>

## II. MEASUREMENT CAMPAIGN

The channel sounder we used to collect measurements has a 60 GHz center frequency and 2 GHz bandwidth. It features a circular array of 16 scalar feed horn antennas at R, each with 18.1 dBi gain and 22.5° beamwidth. To avoid “blind spots,” the angular spacing between the antennas was matched to the beamwidth of the horns. Specifically, the antennas are spaced at 22.5° horizontally; vertically, adjacent antennas are pointed outwards at 0°, and upward at 22.5° toward T. Consequently, the horizontal field-of-view (FoV) of the array is 360° and its vertical FoV is 45°. The T features a similar semispherical array with eight antennas. The 3-D spatial diversity enables the characterization of angle in both azimuth and elevation. An optical cable provides phase synchronization between both ends. A single measurement consists of 128 (16 × 8) complex channel impulse responses electronically switched through each pair of T and R horns, all in just 262 μs.

The 128 CIRs are subsequently synthesized through the SAGE superresolution algorithm to extract channel paths while de-embedding the T and R horn antenna patterns, resulting in  $N$  discrete paths that represent a (quasi) omnidirectional FoV of the channel. The algorithm extracts paths jointly in six domains—complex amplitude ( $\alpha$ ), delay  $\tau$ , and 3-D double-directional angle  $\theta = [\theta^T, \theta^R]$ , where  $\theta^T = [\theta^{T,A}, \theta^{T,E}]$  denotes angle-of-departure (AoD) in azimuth (A) and elevation (E) and  $\theta^R = [\theta^{R,A}, \theta^{R,E}]$  denotes angle-of-arrival (AoA) [27]—ensuring the paths are resolved discretely with high fidelity. In fact, an average measurement error of only 1.95 dB in path gain ( $|\alpha|^2$ ), 0.45 ns in delay, and 2.24° across all four angle dimensions is reported in [28]. Discrete resolution of the paths is assumed when computing all three sparsity metrics in the next section.

The measurements were collected by an autonomous robot at the R end of our channel sounder, equipped with the laser-guided navigational system indoors and differential GPS outdoors, delivering cm-level accuracy. Table I summarizes the parameters of the measurement campaign. A total of 750 large-scale

<sup>2</sup>As a lower DoF means more sparsity, for the DoF cdf, we show (Prob >  $x$ ) as opposed to (Prob ≤  $x$ ), this ensures sparsity increases from left to right for all metrics.

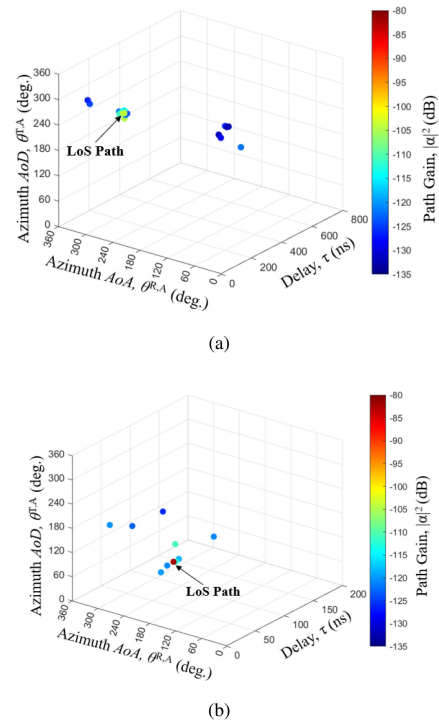


Fig. 1. Paths extracted from a channel measurement in the (a) *Hallway* (least sparse) and (b) *Pathway* (most sparse) environments. Each path is indexed according to delay and azimuth AoD and AoA and coded against path gain in the color bar.

measurements—at different T-R locations throughout—were collected in five different environments: three indoor (*Lobby*, *Lecture Room*, *Hallway*) and two outdoor (*Pathway*, *Street*). Fig. 1 shows the extracted paths from measurements in two different environments.

## III. SPARSITY METRICS

### A. Gini Index

The Gini index is a classic metric for sparsity first presented in [29] to quantify the distribution of wealth within a population. To calculate the Gini index in our application, the vector of  $N$  path gains extracted from a single measurement is sorted in ascending order as  $\mathbf{PG} = [|\alpha_1|^2, |\alpha_2|^2, \dots, |\alpha_N|^2]$ . The Gini index is then calculated as [14], [15], [30]

$$G_{\text{ORIG}} = 1 - 2 \sum_{n=1}^N \left( \frac{\mathbf{PG}(n)}{\|\mathbf{PG}\|_1} \times \frac{N - n + 0.5}{N} \right). \quad (1)$$

Its value ranges from 0 to 1, respectively, indicating that the power is distributed equally among all paths (least sparse) and that the power is distributed all in one path (most sparse). In economics, the Gini index has been shown to have a significant bias, in that it underrepresents sparsity for small sample sets [31], [32]. While this bias is well discussed in economics, it has not yet been considered in application to wireless channel sparsity [14], [15], [33]. In Section IV-A, we show that bias does, indeed, significantly impact wireless channels and to eliminate it, we propose applying the simple correction from [31]

$$G = G_{\text{ORIG}} \cdot \frac{N}{N - 1}. \quad (2)$$

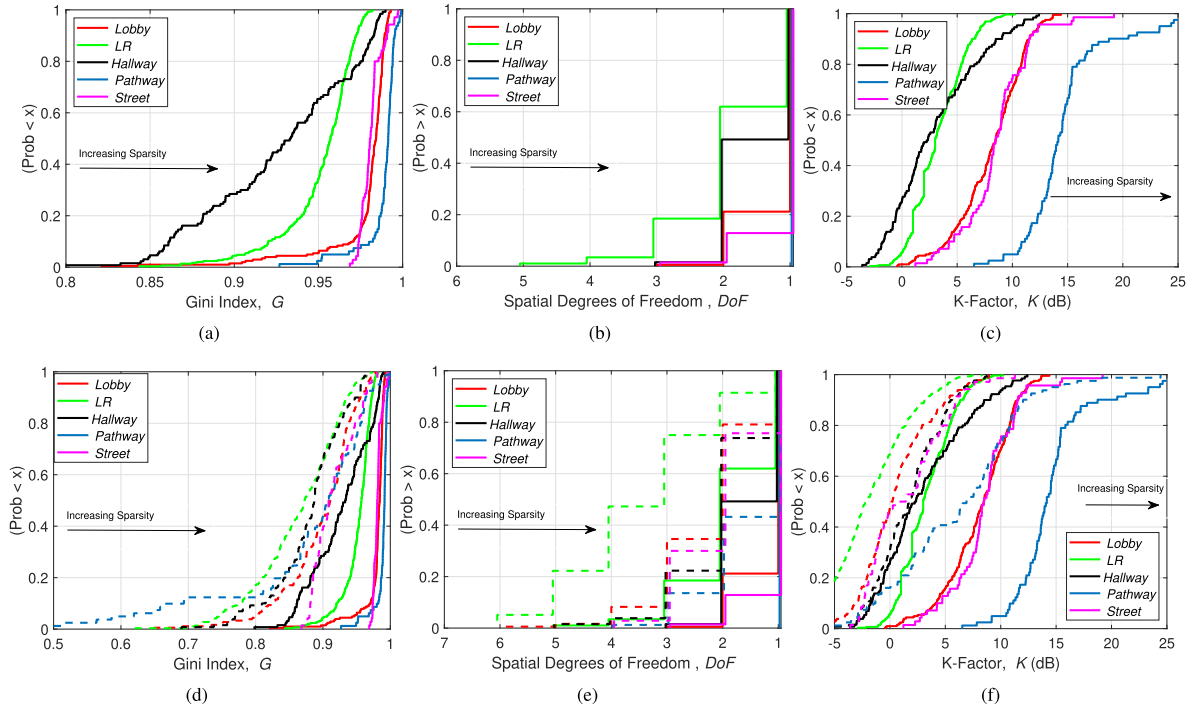


Fig. 2. CDFs of sparsity metrics for each environment. LoS scenarios: (a) Gini index. (b) DoF. (c) Rician  $K$ -factor. OLoS scenarios (dotted lines) and LoS are shown for comparison (solid lines): (d) Gini index. (e) DoF. (f) Rician  $K$ -factor.

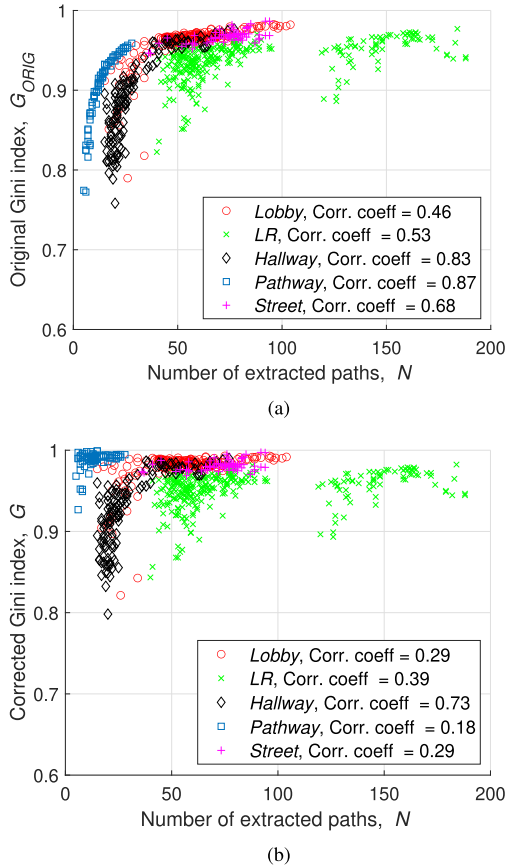


Fig. 3. Correlation between the Gini index and the number of extracted paths per measurement. The 1800 channel measurements are clustered in color per environment. (a) Original Gini index. (b) Corrected Gini index [31].

Henceforth, any mention of the Gini index refers to the corrected version  $G$ , and in Section IV-A, we substantiate the validity of the correction through our measurements.

### B. Spatial DoF

The spatial DoF is defined as the number of antennas in a MIMO system that is exploited for spatial multiplexing [14], [15], [22], [34]. A large DoF indicates multipath richness and so proxies as a metric for sparsity [14], [15]. The DoF is computed as the rank of the channel correlation matrix  $\mathbf{H}\mathbf{H}^\dagger$ :

$$\text{DoF} = \text{rank}(E[\mathbf{H}\mathbf{H}^\dagger]) \quad (3)$$

where  $\mathbf{H}$  is the channel matrix of the MIMO system and  $\dagger$  is the Hermitian. In both [14], [15] and [34], the rank is estimated as the number of eigenvalues/eigenchannels of  $\mathbf{H}\mathbf{H}^\dagger$  that are within 20 dB of the maximum eigenvalue. We also used 20 dB due to its prevalence in the literature.

The MIMO system we model is a  $\sqrt{P} \times \sqrt{P}$  planar phased array at both T and R with half-wavelength ( $\frac{\lambda}{2}$ ) spacing between antennas. The array steering vector is given by  $S_i = \frac{1}{\sqrt{P}} e^{-j \frac{2\pi}{\lambda} (\cos\theta^A \cos\theta^E \cdot x_i + \sin\theta^A \cos\theta^E \cdot y_i)}$ , where  $x_i$  and  $y_i$  are the positions of antenna  $i$  and  $\theta = [\theta^A, \theta^E]$  is the steering angle. Since  $\text{DoF} \leq \min(P, N)$ ,  $P = 256$  was selected so that it is larger than the maximum  $N$  (194) across all measurements in all environments. The  $ij$ th entry of the  $P \times P$  channel matrix  $\mathbf{H}$  is given as [27]

$$h_{ij} = \sum_{n=1}^N \alpha_n \cdot S_i^T(\theta_n^T) \cdot S_j^R(\theta_n^R) \quad (4)$$

TABLE II  
PEARSON CORRELATION COEFFICIENT BETWEEN METRICS PER ENVIRONMENT

	<i>Lobby</i>	<i>LR</i>	<i>Hallway</i>	<i>Pathway</i>	<i>Street</i>	Avg.
DoF versus $G$	0.62	0.58	0.44	N/A	0.53	0.53
$K$ versus $G$	0.61	0.50	0.45	0.51	0.61	0.53
$K$ versus DoF	0.68	0.48	0.85	N/A	0.71	0.68

where  $S_i^T$  and  $S_j^R$  are the steering vectors of the T and R antennas, respectively.

### C. Rician $K$ -Factor

In [14] and [15], the Rician  $K$ -factor was first proposed as a metric for sparsity. The  $K$ -factor is computed as the ratio of the power of the strongest path to the total power of all other paths

$$K = \frac{PG_N}{PG_1 + PG_2 + \dots + PG_{N-1}}. \quad (5)$$

A larger  $K$ -factor indicates a sparser channel with greater power in the dominant path and a smaller  $K$ -factor indicates decreasing sparsity with a greater amount of power in the secondary paths.

## IV. RESULTS AND CONCLUSIONS

### A. Comparing Sparsity Metrics

The cumulative distribution function (cdf) for the three sparsity metrics was compiled across all the measurements per environment and are plotted in Fig. 2(a)–(c) with increasing sparsity from left to right for easy comparison. All three metrics rank the sparsity of the environments in similar order, indicating high correlation between them; this is substantiated in Table II<sup>3</sup>, which tabulates the Pearson correlation coefficient between the three metrics per environment—most are above 0.5. The average values in Table II show that the strongest correlations are observed for  $K$  versus DoF; the weaker correlations of these two versus  $G$  are expected since  $G$  quantifies a different property of the channel, namely the distribution of power among the paths, whereas the  $K$  and DoF, respectively, quantify the dominance of the strongest path and the dominance of the few strongest paths with respect to the others.

To demonstrate the importance of the corrected Gini index, Fig. 3(a) and (b), respectively, shows the original and corrected Gini index versus  $N$  for all 750 measurements, clustered in a different color per environment; the legend displays the correlation coefficient between the index and  $N$ . The *Pathway* is the environment where the least number of paths is extracted on average (15); its bias due to small sample sets is apparent in Fig. 3(a), in that  $G_{\text{ORIG}}$  increases notably as a function of  $N$ . This is supported by a high correlation coefficient of 0.87. The functional dependence retreats as  $N$  exceeds 20, meaning that the bias is less severe thereafter; in fact, very little bias is apparent for the *Lecture Room*, where  $N$  is always in excess of 40. When the bias correction [31] is applied in Fig. 3(b), the correlation coefficient drops for all environments, in particular in the *Pathway*, down to 0.18. A small drop is observed only in the *Hallway*: In this environment, low  $N$  corresponds to when R is far down the hallway, where most ambient paths have died down and the only ones detected—the LoS path, the paths waveguided

<sup>3</sup>As the DoF for all locations in the *Pathway* environment is 1, the correlation coefficient is undefined.

along the ceiling, floor, and walls, and the strong reflection from the back wall—are comparable in strength; hence, the channel is inherently less sparse as indicated by the Gini index. This is well illustrated in Fig. 1(a), where three strong reflected paths are detected with power comparable to the LoS path.

### B. Comparing Indoors Versus Outdoors

While direct comparison to other literature is imperfect due to differences in environments and measurement equipment, the reported median values of  $G$ , DoF, and  $K$  in [14] and [15] for a street environment in LoS conditions at 5.9 GHz are 0.63, 6, and 2.2 dB, respectively. The median values for our *Street* environment (LoS) are 0.97, 1, and 8.2 dB, suggesting that the mmWave channel is, indeed, much sparser than the microwave channel. Indoor measurements under LoS conditions at 5.2 GHz in [18], where only the DoF is reported, show a median value of 5, which is significantly less sparse than the median values reported for our indoor environments: 1 for *Lobby* and 2 for *Lecture Room* and *Hallway*.

The *Hallway* is the least sparse environment per all three metrics, returning the lowest median  $G$  (0.93), the highest median DoF (3), and the lowest median  $K$  (2.4 dB). The reduced sparsity compared to the other environments stems from the previously discussed waveguiding effect and back wall reflection. The *Lecture Room* is an enclosed environment with multiple scatterers such as chairs, tables, and glass doors, providing many strong specular paths; hence, more multipath richness compared to the open *Lobby* with few scattering objects and the latter is more sparse. The lack of buildings and other structures in the *Pathway* environment [35, Fig. 1] coupled with significantly wider dimensions, translates to reflections with longer path lengths relative to the LoS path—resulting in fewer paths with significant power and extreme sparsity. While the LoS still dominates in the *Street* environment, the denser urban environment contains more buildings in addition to cars and other objects, acting as scatterers between T and R and resulting in stronger reflections and less sparsity, with all three metrics returning similar sparsity readings to the *Lobby*.

### C. Comparing LoS Versus OLoS

By virtue of weak diffraction in the mmWave channel, the high degree of sparsity observed thus far can be attributed to concentration of most R power in the LoS path, which is always detected thanks to the measurement conditions. In the field, however, the LoS path will often be blocked by humans, buildings, foliage, etc., which can inflict penetration losses up to 65 dB [36], creating OLoS conditions. To investigate sparsity in OLoS conditions, we removed the LoS path—clearly identifiable as the strongest and first path, as shown in Fig. 1(a) and (b)—from the extracted paths in postprocessing. We then recompiled the cdfs, shown in Fig. 2(d)–(f) side-by-side the original cdfs. In comparing OLoS versus LoS, we see that sparsity drops notably in all environments and per all three metrics, in particular, the median values averaged across all environments go from  $G = 0.96$ , DoF = 1.4,  $K = 7.3$  dB in LoS to  $G = 0.89$ , DoF = 2.2,  $K = 1.6$  dB in OLoS. Albeit, a high level of sparsity is still observed in OLoS due to one or two dominant reflections; in fact, the metrics we report in OLoS at mmWave are still sparser than the metrics reported in LoS in Section IV-B at microwave. This highlights that, in absence of diffracted paths, reflections are an important propagation mechanism at mmWave frequencies [1].

## REFERENCES

- [1] M. Shafi et al., "Microwave vs. millimeter-wave propagation channels: Key differences and impact on 5G cellular systems," *IEEE Commun. Mag.*, vol. 56, no. 12, pp. 14–20, Dec. 2018.
- [2] M. Shafi et al., "5G: A tutorial overview of standards, trials, challenges, deployment, and practice," *IEEE J. Sel. Areas Commun.*, vol. 35, no. 6, pp. 1201–1221, Jun. 2017.
- [3] M. K. Samimi and T. S. Rappaport, "3-D millimeter-wave statistical channel model for 5G wireless system design," *IEEE Trans. Microw. Theory Techn.*, vol. 64, no. 7, pp. 2207–2225, Jul. 2016.
- [4] C. Qi, Y. Huang, S. Jin, and L. Wu, "Sparse channel estimation based on compressed sensing for massive MIMO systems," in *Proc. IEEE Int. Conf. Commun.*, 2015, pp. 4558–4563.
- [5] P. Wang, M. Pajovic, P. V. Orlik, T. Koike-Akino, K. J. Kim, and J. Fang, "Sparse channel estimation in millimeter wave communications: Exploiting joint AoD-AoA angular spread," in *Proc. IEEE Int. Conf. Commun.*, 2017, pp. 1–6.
- [6] A. Alkhateeb, G. Leus, and R. W. Heath, "Compressed sensing based multi-user millimeter wave systems: How many measurements are needed?," in *Proc. IEEE Int. Conf. Acoust., Speech, Signal Process.*, 2015, pp. 2909–2913.
- [7] C. Gentile et al., "Millimeter-wave channel measurement and modeling: A NIST perspective," *IEEE Commun. Mag.*, vol. 56, no. 12, pp. 30–37, Dec. 2018.
- [8] S. Deng, G. R. MacCartney, and T. S. Rappaport, "Indoor and outdoor 5G diffraction measurements and models at 10, 20, and 26 GHz," in *Proc. IEEE Glob. Commun. Conf.*, 2016, pp. 1–7.
- [9] R. Charbonnier et al., "Calibration of ray-tracing with diffuse scattering against 28-GHz directional urban channel measurements," *IEEE Trans. Veh. Technol.*, vol. 69, no. 12, pp. 14264–14276, Dec. 2020.
- [10] J. Senic, C. Gentile, P. B. Papazian, K. A. Remley, and J.-K. Choi, "Analysis of E-band path loss and propagation mechanisms in the indoor environment," *IEEE Trans. Antennas Propag.*, vol. 65, no. 12, pp. 6562–6573, Dec. 2017.
- [11] H. Zhao et al., "28 GHz millimeter-wave cellular communication measurements for reflection and penetration loss in and around buildings in New York city," in *Proc. IEEE Int. Conf. Commun.*, 2013, pp. 5163–5167.
- [12] C. Lai, R. Sun, C. Gentile, P. B. Papazian, J. Wang, and J. Senic, "Methodology for multipath-component tracking in millimeter-wave channel modeling," *IEEE Trans. Antennas Propag.*, vol. 67, no. 3, pp. 1826–1836, Mar. 2019.
- [13] R. W. Heath, N. González-Prelcic, S. Rangan, W. Roh, and A. M. Sayeed, "An overview of signal processing techniques for millimeter wave MIMO systems," *IEEE J. Sel. Topics Signal Process.*, vol. 10, no. 3, pp. 436–453, Apr. 2016.
- [14] H. Zhang, R. He, B. Ai, S. Cui, and H. Zhang, "Measuring sparsity of wireless channels," *IEEE Trans. Cogn. Commun. Netw.*, vol. 7, no. 1, pp. 133–144, Mar. 2021.
- [15] R. He, B. Ai, G. Wang, M. Yang, C. Huang, and Z. Zhong, "Wireless channel sparsity: Measurement, analysis, and exploitation in estimation," *IEEE Wireless Commun.*, vol. 28, no. 4, pp. 113–119, Aug. 2021.
- [16] W. Weichselberger, M. Herdin, H. Ozcelik, and E. Bonek, "A stochastic MIMO channel model with joint correlation of both link ends," *IEEE Trans. Wireless Commun.*, vol. 5, no. 1, pp. 90–100, Jan. 2006.
- [17] A. M. Sayeed and V. Raghavan, "Maximizing MIMO capacity in sparse multipath with reconfigurable antenna arrays," *IEEE J. Sel. Topics Signal Process.*, vol. 1, no. 1, pp. 156–166, Jun. 2007. [Online]. Available: <https://ieeexplore-ieee-org.ezproxy.canterbury.ac.nz/abstract/document/4200712>
- [18] M. Matthaiou, A. M. Sayeed, and J. A. Nossek, "Sparse multipath MIMO channels: Performance implications based on measurement data," in *Proc. IEEE 10th Workshop Signal Process. Adv. Wireless Commun.*, 2009, pp. 364–368.
- [19] P. Tang, J. Zhang, M. Shafi, P. A. Dmochowski, and P. J. Smith, "Millimeter wave channel measurements and modelling in an indoor hotspot scenario at 28 GHz," in *Proc. IEEE 88th Veh. Technol. Conf.*, 2018, pp. 1–5.
- [20] X. Yin, C. Ling, and M.-D. Kim, "Experimental multipath-cluster characteristics of 28-GHz propagation channel," *IEEE Access*, vol. 3, pp. 3138–3150, 2015.
- [21] J. Ko et al., "Millimeter-wave channel measurements and analysis for statistical spatial channel model in in-building and urban environments at 28 GHz," *IEEE Trans. Wireless Commun.*, vol. 16, no. 9, pp. 5853–5868, Sep. 2017.
- [22] M. R. Akdeniz et al., "Millimeter wave channel modeling and cellular capacity evaluation," *IEEE J. Sel. Areas Commun.*, vol. 32, no. 6, pp. 1164–1179, Jun. 2014.
- [23] ETSI TR 138 901 V14.3.0, 5G; Study on Channel Model for Frequencies From 0.5 to 100 GHz, 3GPP, Industry Standard TR 38.901 V14.3.0, Jan. 2018. [Online]. Available: [https://www.etsi.org/deliver/etsi\\_tr/138900/138999/138901/14.03.00\\_60/tr\\_138901v140300p.pdf](https://www.etsi.org/deliver/etsi_tr/138900/138999/138901/14.03.00_60/tr_138901v140300p.pdf)
- [24] N. Varshney, J. Wang, C. Lai, C. Gentile, R. Charbonnier, and Y. Corre, "Quasi-deterministic channel propagation model for an urban environment at 28 GHz," *IEEE Antennas Wireless Propag. Lett.*, vol. 20, no. 7, pp. 1145–1149, Jul. 2021.
- [25] Z. Pi and F. Khan, "An introduction to millimeter-wave mobile broadband systems," *IEEE Commun. Mag.*, vol. 49, no. 6, pp. 101–107, Jun. 2011.
- [26] W. U. Bajwa, J. Haupt, A. M. Sayeed, and R. Nowak, "Compressed channel sensing: A new approach to estimating sparse multipath channels," *Proc. IEEE*, vol. 98, no. 6, pp. 1058–1076, Jun. 2010.
- [27] S. Blandino, J. Senic, C. Gentile, D. Caudill, J. Chuang, and A. Kayani, "Markov multi-beamtracking on 60 GHz mobile channel measurements," *IEEE Open J. Veh. Technol.*, vol. 3, pp. 26–39, 2021.
- [28] R. Sun et al., "Design and calibration of a double-directional 60 GHz channel sounder for multipath component tracking," in *Proc. 11th Eur. Conf. Antennas Propag.*, 2017, pp. 3336–3340.
- [29] C. Gini, "Measurement of inequality of incomes," *Econ. J.*, vol. 31, no. 121, pp. 124–126, 1921. [Online]. Available: <https://www.jstor.org/stable/2223319>
- [30] N. Hurley and S. Rickard, "Comparing measures of sparsity," *IEEE Trans. Inf. Theory*, vol. 55, no. 10, pp. 4723–4741, Oct. 2009.
- [31] G. Deltas, "The small-sample bias of the Gini coefficient: Results and implications for empirical research," *Rev. Econ. Statist.*, vol. 85, no. 1, pp. 226–234, Feb. 2003, doi: [10.1162/rest.2003.85.1.226](https://doi.org/10.1162/rest.2003.85.1.226).
- [32] T. Van Ourti and P. Clarke, "A simple correction to remove the bias of the Gini coefficient due to grouping," *Rev. Econ. Statist.*, vol. 93, no. 3, pp. 982–994, Aug. 2011, doi: [10.1162/REST\\_a\\_00103](https://doi.org/10.1162/REST_a_00103).
- [33] N. Hurley, S. Rickard, and P. Curran, "Parameterized lifting for sparse signal representations using the Gini index," in *Proc. Signal Process. Adaptive Sparse Structured Representations*, Rennes, France, Nov. 2005.
- [34] K. Haneda et al., "Measurement-based analysis of spatial degrees of freedom in multipath propagation channels," *IEEE Trans. Antennas Propag.*, vol. 61, no. 2, pp. 890–900, Feb. 2013.
- [35] S. Y. Jun et al., "Quasi-deterministic channel propagation model for 60 GHz urban WiFi access from light poles," *IEEE Antennas Wireless Propag. Lett.*, vol. 21, no. 8, pp. 1517–1521, Aug. 2022.
- [36] S. Y. Jun et al., "Penetration loss at 60 GHz for indoor-to-indoor and outdoor-to-indoor mobile scenarios," in *Proc. 14th Eur. Conf. Antennas Propag.*, 2020, pp. 1–5.